Restoring Adiabaticity Around an Exceptional Point in a Two-Mode System

Vishnu Chavva[1] and Hugo Ribeiro[1]

[1] *Department of Physics and Applied Physics, University of Massachusetts Lowell, Lowell, MA 01854, USA*

Non-Hermitian Hamiltonians (NHH) contain a variety of special topological properties that are relevant to improving robustness against noise and imprecisions in quantum state transfer. To generate such operations one needs to adiabatically evolve the system around an exceptional point (EP) along a control loop in parameter space. However, since the adiabatic theorem is broken for NHHs, this is impossible to reproduce dynamically. Here we propose a general strategy for resolving eigenstate swapping (and by association eigenvalue braiding) by adapting well known Hermitian shortcuts-to-adiabaticity (STAs) for a NHH using a dressed state approach. However, we find that NHH STAs require special considerations due to branch cuts present in the complex eigenspectrum, which may produce discontinuous, and thereby unusable control fields. We account for this and show that our STAs can restore adiabaticity even in the non-adiabatic regime. We also propose a new STA which reduces the amplitude of the control fields when compared to well-known STAs, while adhering to the experimental constraints of the system. Finally, we perform a robustness check and find a parameter loop time regime in which the STAs produced the desired state swap despite small parameter imprecisions.

I. INTRODUCTION

Any approach to implement quantum gates relies on applying time-dependent control fields such that the corresponding time-dependent Hamiltonian generates the desired unitary evolution. Regardless of the setting, the generated evolution must be resilient against both coherent errors, arising from unwanted interactions to leakage states or non-adiabatic processes, and incoherent errors due to coupling to a bath. Taking advantage of control frameworks [1–10], it is possible to find control sequences that mitigate coherent errors and accelerate quantum dynamics. These allow one to generate faster, high-fidelity gates from a unitary point of view. If the resulting gate time is much shorter than the characteristic decoherence time, then the evolution is also partially protected against incoherent errors since the bath will not have enough time to fully disrupt the quantum dynamics. Methods that fully protect quantum dynamics against incoherent errors are yet to be developed.

An attractive strategy is to exploit topological properties to make a quantum system robust against noise and imprecisions [11–19]. In the context of quantum gates one can use the interplay between dissipative and coherent dynamics to realize quantum operations that are determined by a topological property of the underlying equations of motion governing the dynamics. Generically, the equations of motion describing an open quantum system take the form $\dot{\boldsymbol{c}}(t) = \mathbf{D}\boldsymbol{c}(t)$, with $\boldsymbol{c}(t)$ a complex vector describing the state of the system and $\mathbf{D}$ can either be a Liouvillian superoperator $\ell(t)$ or a non-Hermitian Hamiltonian operator $\mathbf{H}(t)$. The spectrum of $\mathbf{D}$ as a function of the parameters of the system is in general complex and possesses branch singularities called exceptional points (EP) where eigenvalues become degenerate and $\mathbf{D}$ cannot be diagonalized. The presence of exceptional points in the spectrum of $\mathbf{D}$ yields a non-trivial spectral topology that can be leveraged to realize topological operations. From topological considerations only, varying the systems parameters in a closed loop around an exceptional point leads to a topological operation that corresponds to an eigenstate swap [20, 21].

To generate such a topological operation in practice one needs to adiabatically evolve the system in time along a control loop that encircles an exceptional point in parameter space. However, because the adiabatic theorem is violated for non-Hermitian systems, one cannot adiabatically transport all of the eigenstates, but only the eigenstate that is least damped [22, 23]. As a consequence, adiabatically encircling exceptional points with a control loop does not allow one to realize a state swap, but rather a non-reciprocal state transfer; independently of which eigenstate is initially prepared, the system always ends up in the least damped eigenstate [22, 23]. This behavior has been most studied and observed when $\mathbf{D}$ is a two-dimensional non-Hermitian Hamiltonian [24–26]. While this seems to put an end to any prospect of realizing any topological operation (or gate), inspiration from the field of shortcuts-to-adiabaticity provides a path forward to design control sequences that generate an evolution that mimics adiabatic dynamics.

In this work, we present a highly general strategy to construct shortcuts-to-adiabaticity for non-Hermitian Hamiltonians based on the dressed state scheme [27]. While it would appear that extending the dressed state approach to shortcuts-to-adiabaticity for non-Hermitian Hamiltonians would be a straightforward generalization, the non-trivial spectral topology of non-Hermitian Hamiltonians, and in particular the presence of singularities, prohibits one to use the same strategy as in the Hermitian case. The starting point of the dressed state approach is the time-dependent Hamiltonian $\hat{H}(t)$ for which one has designed an adiabatic protocol of duration t_f. When the gap ΔE between energy eigenstates is much larger than $1/t_\mathrm{f}$, i.e., $\Delta E t_\mathrm{f} \gg 1$, an almost perfect adiabatic evolution can be achieved: The system will remain at all times in the instantaneous eigenstate $|\psi_n(t)\rangle$, if $|\psi_n(t=0)\rangle$ is initially prepared. Thus, the adiabatic evo-

[HR 1] cite

[HR 2] comment on PT symmetry

[HR 3] cite

[HR 4] cite

[HR 5] cite

[HR 6] cite

lution generated by $\hat{H}(t)$ allows one to map $|\psi_n(t=0)\rangle$ to $|\psi_n(t=t_\mathrm{f})\rangle$. If one is only interested in this specific mapping and does not which to keep the system at all times in $|\psi_n(t)\rangle$, then the dressed approach allows one to find a modification of the adiabatic protocol such that the generated evolution maps $|\psi_n(t=0)\rangle$ to $|\psi_n(t=t_\mathrm{f})\rangle$ independently of the magnitude of $\Delta E t_\mathrm{f}$.

In practice, the modified control sequence is found by choosing a unitary transformation $S_\mathrm{dr}(t)$ that dresses the instantaneous eigenstates and a control Hamiltonian $\hat{W}(t)$ that only cancels unwanted transitions between dressed instantaneous eigenstates. While in the Hermitian case the choice of dressing is completely arbitrary, which allows one to pick a dressing that leads to a $\hat{W}(t)$ compatible with the constraints of the physical system at hand, in the non-Hermitian case the presence of singularities in the spectrum of $\mathbf{H}(t)$ restricts the possible dressing transformations. Moreover, and in stark contrast to the Hermitian case, a particular dressing will not always result in a family of solutions to the control problem: depending on the duration t_f of the initial protocol encircling the exceptional point, a specific dressing transformation might not yield a modified control sequence that generates the desired dynamics.

Our work establishes simple criteria based on the spectral topology of $\mathbf{H}$ that allow one to rule out dressing transformations as well as identifying the durations for which a specific dressing predicts a valid shortcut to adiabaticity. We illustrate our formalism by designing control sequences that yield eigenvalue braiding (topological state swap) for a two-mode system and study their robustness against parameter uncertainties. In stark contrast to the Hermitian case, we find that non-Hermitian shortcuts to adiabaticity are extremely sensitive to parameter variations, especially in the long time-limit, and propose a method to find robust sequences that can be implemented experimentally.

The idea of using shortcuts to adiabaticity in the context of non-Hermitian dynamics is not new, with earlier works addressing the generalization of transitionless driving to non-Hermitian Hamiltonians and how one could engineer decay to cancel nonadiabatic transitions in the context of state transfer. These approaches focus on the design of shortcuts to adiabaticity away from the spectrum singularities. As we discussed above, our approach is significantly different from these strategies, since it allows one to find shortcuts to adiabaticity when encircling exceptional points.

The remainder of this paper is organized as follows: In Sec.XXX we define...

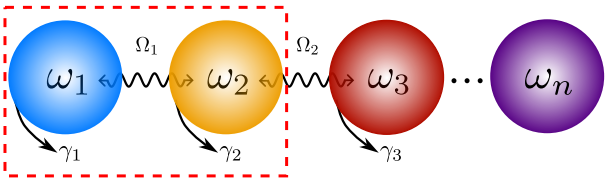

Figure 1. N-coupled modes with local dissipation. The dissipative evolution of the system can be described by an effective non-Hermitian Hamiltonian with corresponding coupling strengths Ω_n and dissipation rates γ_n.

II. PRELIMINARIES

A. Spectral flow and topological operations

We consider the generic non-Hermitian Hamiltonian

$$H = H(\boldsymbol{p}), \tag{1}$$

where $\boldsymbol{p} = \{p_1, \ldots, p_i, \ldots, p_n\}$ is a shorthand notation to indicate that H depends on n parameters that can be externally varied. The right eigenstates of Eq. (1) and corresponding right eigenvalues, defined by

$$H(\boldsymbol{p})|\psi_j(\boldsymbol{p})\rangle = \lambda_j(\boldsymbol{p})|\psi_j(\boldsymbol{p})\rangle, \tag{2}$$

where

$$|\psi_j(\boldsymbol{p})\rangle = \sum_{\beta=1}^{n} c_\beta(\boldsymbol{p})|\beta\rangle, \tag{3}$$

and $\{|\beta\rangle\}_{\beta=1}^n$ is a basis of the Hilbert space associated to $H(t)$, both functions of $\boldsymbol{p}$. Generically, as one varies $\boldsymbol{p}$, the spectrum of H becomes degenerate. At the degeneracy points, which we denote by $\boldsymbol{p} = \boldsymbol{p}_{m_k}^{(\mathrm{EP}_k)}$, k eigenvalues and eigenvectors coalesce and H is non-diagonalizable. These singularities in the spectrum of $H(\boldsymbol{p})$ are known as Exceptional Points (EPs). For order k, there are M_k EPs, i.e., $m_k \in 1, \ldots, M_k$. The subspace defined by $\{\boldsymbol{p} = \boldsymbol{p}_{m_k}^{(\mathrm{EP}_k)}\}_{m_k=1}^{M_k}$ and its complementary manifold $\boldsymbol{p}$s (where H is diagonalizable) may form non-trivial topological spaces [21, 28–34].

We can then define closed contours in $\boldsymbol{p}$s, $\gamma(\varepsilon) = [p_1(\varepsilon), \ldots, p_n(\varepsilon)]$ with $\varepsilon \in [0,1]$, that wind around the EPs such that $H[\boldsymbol{p}(\varepsilon=0)] = H[\boldsymbol{p}(\varepsilon=1)]$. The eigenvalues as a function of $\boldsymbol{p}(\varepsilon)$ will therefore trace braids of N strands where $N \leq n$. A subset of these strands will cross each other such that

$$\lambda_j[\boldsymbol{p}(\varepsilon=0)] \to \lambda_j[\boldsymbol{p}(\varepsilon=1)] = \lambda_{\sigma(j)}[\boldsymbol{p}(\varepsilon=0)], \tag{4}$$

where $\sigma(j)$ is a permutation of the elements of $j \in \{1, \ldots, N\}$. This operation is known as eigenvalue braiding, in which $\lambda_j[\boldsymbol{p}(\varepsilon=1)] = \lambda_{i\neq j}[\boldsymbol{p}(\varepsilon=0)]$. The associated eigenstate permutation can then be defined by a topological permutation operator

$$P_{\sigma(j),j} = \exp[i\phi_{\sigma(j),j}]|\psi_{\sigma(j)}\rangle. \tag{5}$$

[VC 1] curl brackets bc list of parameters?

[VC 2] does "N" here just equal order "k"?

[VC 3] cite

[HR 7] cite erry, Demirlak, etc

[HR 8] cite banez 2011

[HR 9] cite brosov 2013, heck more!

[HR 10] Discuss Nori paper?

In particular, we can say that σ is the permutation defined by γ with the same base point on along the parameter loop belonging to the same homotopy class ℓ. For our discussion, there are two classes of ℓs: contours that do and do not encircle the EP. We are mainly interested in the former: parameter loops that cross the branch cut present in the complex spectrum of $\boldsymbol{p}$s (for non-Hermitian Hamiltonians, $\lambda_j \in \mathbb{C}$). The eigenvalues λ_j along these loops follow the permutation in Eq. (4) that define a group identical to the Artin braid group B_n [35].

To understand this, let us first consider the simple case $n = 2$ and that a subset of parameters $\{p_k\}_k \subseteq \boldsymbol{p}$ is varied along a closed contour while the complementary subset $\overline{\{p_l\}}_l$ is kept constant. We further assume that the control loop $\gamma(t) = \{p_k(t)\}_k$ encloses an EP of $H(t)$. Recalling that for a two-dimensional non-Hermitian operator the general expression for the eigenvalues is $\lambda_\pm(t) = \mathrm{Tr}[H(t)] \pm \sqrt{f[\boldsymbol{p}(t)]}$ with $f[\boldsymbol{p}(t)] \in \mathbb{C}$, that the location of the EPs is determined by $f[\boldsymbol{p}(t)] = 0$, and that the complex square root function $\sqrt{f[\boldsymbol{p}(t)]}$ can only be defined on the domain $\mathbb{C} \setminus \mathbb{R}^-$ to be holomorphic, we conclude that $\lambda_\pm(t)$ is not differentiable with respect to $\{p_k\}_k$ along $\gamma(t)$. For a closed control loop encapsulating an EP, the identity $f[\boldsymbol{p}(0)] = f[\boldsymbol{p}(t_0)]$ implies that $f[\boldsymbol{p}(t)]$ must cross $\mathbb{R}^-$. The same argument can be extended to n-dimensional system by noticing that around an EP of degree k, the eigenvalues asymptotically behave like the kth root, i.e., $\lambda_j \sim \sqrt[k]{f[\boldsymbol{p}(t)]}$ [36].

[VC 4] can you show me how you get this? and how =Arg[λ]?

B. "Adiabatic" Evolution and Holomorphic Change of Frame Operators

To experimentally reproduce these phenomena requires varying $\boldsymbol{p}$ along a control loop in time such that $\varepsilon \to \varepsilon(t)$, thus Eq. (1) becomes explicitly time dependent, and obeys the Schrödinger-like equation of motion for the flow operator $\Phi(t)$ [equivalent to the unitary evolution operator $\hat{U}(t)$]

$$i\dot{\Phi}(t) = H(t)\Phi(t), \tag{6}$$

with $\Phi(0) = \mathbb{1}$. The flow $\Phi(t)$ allows one to find the state of the system at time t, only if one knows the state at time $t = 0$ through the relation $|s(t)\rangle = \Phi(t)|s(0)\rangle$. In order to generate $P_{\sigma_\gamma(j),j}$, $H(t)$ must be varied adiabatically. However, this is impossible for non-Hermitian systems; when dynamically encircling an EP, only the least damped eigenstate of $H(t)$ can evolve adiabatically [36–39]. The permutation σ is therefore no longer valid.

This behavior is best understood in the frame of instantaneous eigenstates where $H(t)$ is diagonal at each instant of time t, diagonalized using the change of frame operator given by

$$S_{\mathrm{ad}}[\boldsymbol{p}(t)] = \sum_{j=1}^{n} |\psi_j[\boldsymbol{p}_i(t)]\rangle\langle k_j|, \tag{7}$$

In the adiabatic frame, the non-Hermitian Hamiltonian governing the dynamics is given by

$$\begin{aligned} H_{\mathrm{ad}}(t) &= S_{\mathrm{ad}}^{-1}(t)H(t)S_{\mathrm{ad}}(t) - iS_{\mathrm{ad}}^{-1}(t)\dot{S}_{\mathrm{ad}}(t) \\ &= \sum_j \lambda_j(t)|\psi_j\rangle\langle\psi_j| - iS_{\mathrm{ad}}^{-1}(t)\sum_{j=1}^{n}\frac{\partial S_{\mathrm{ad}}(t)}{\partial \boldsymbol{p}_j}\dot{\boldsymbol{p}}_j(t), \end{aligned} \tag{8}$$

where we use Newton's notation for time differentiation, $\dot{x}(t) = \mathrm{d}x(t)/\mathrm{d}t$ and omitted the dependence on $\boldsymbol{p}$ for simplicity.

To correctly define Eq. (8) one must construct a change of frame operator $S_{\mathrm{ad}}(t)$ that is holomorphic everywhere except at the location of the EPs, which are singularities in the spectrum of $H(t)$. This can be done by defining both the expansion coefficients of $|\psi_j(t)\rangle$ [see Eq. (3) and $\lambda_j(t)$, which are multivariate functions of $\boldsymbol{p}$, on their associated Riemann surface [40]. In practice, the expansion coefficient of $|\psi_j(t)\rangle$ will turn out to be holomorphic, if one first defines $\lambda_j(t)$ on its Riemann surface and then solves for $|\psi_j(t)\rangle$. We show an explicit example of this procedure in Sec. III.

However despite constructing holomorphic operators, one cannot ensure that the braid group determined by adiabatically evolving $H(t)$ is isomorphic to the braid group given in the static case for the same class of loops ℓ (disregarding parameterization). This is due to the operator $-iS_{\mathrm{ad}}^{-1}(t)\dot{S}_{\mathrm{ad}}(t)$ [see Eq. (8)], which describes the non-inertial coupling between the instantaneous eigenstates $|\psi_j\rangle$; since $H(t)$ is explicitly time-dependent its instantaneous eigenstates are not stationary. The non-inertial term accounts for a coupling between the instantaneous eigenstates of H_{sym} that induces non-adiabatic transitions. These transitions, in contrast to the Hermitian case, prevent the system from following adiabatic dynamics even in the long-time limit, despite the non-inertial term scaling as $1/t_0$. For non-Hermitian systems, the condition $\langle i|-iS_{\mathrm{ad}}^{-1}\dot{S}_{\mathrm{ad}}|j\rangle/(\lambda_i-\lambda_j)$ is not sufficient to determine if the adiabatic approximation can be made.

[VC 5] where does this come from?

We again refer to the simple case of $n = 2$ to better understand these non-reciprocal dynamics. The non-inertial term generates amplification/damping according to the sign of the imaginary parts of $\lambda_\pm$ ("+" amplification, "-" damping). This implies that the dynamics generated by the diagonal part of H_{ad} [see Eq.(8)] leads to amplitude amplification (damping) for the eigenmode associated to λ_+ (λ_-) given by $|+\rangle$ ($|-\rangle$), and referred to as the gain (loss) mode. The non-inertial term enables amplitude transitions between the eigenmodes such that initializing the system in $|-\rangle$ will result in a "small" amount of amplitude being transferred to $|+\rangle$, which will therefore be amplified due to the complex eigenvalues. When transition from $|+\rangle$ to $|-\rangle$ the reverse is true, as the amplitude is damped instead. The longer the loop time ($t_0 \to \infty$), the greater the amplification/damping. Thus, at $t = t_0$, most of the "energy" is stored in the gain mode, resulting in a violation of the adiabatic theorem. Accordingly, λ_+ will trace its braid, λ_- will not. These

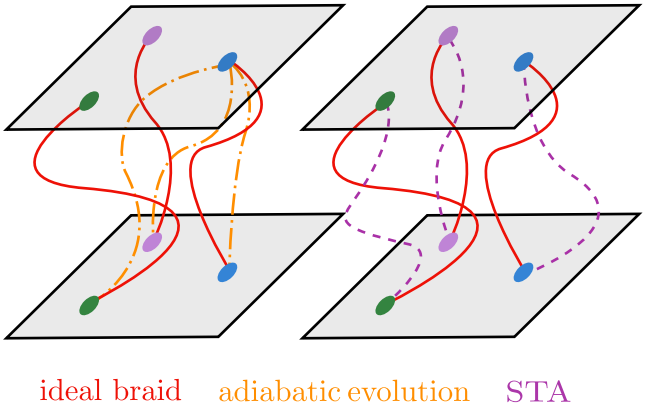

Figure 2. Schematic representations of the eigenvalues braids traced by a choice of contour $\gamma(\varepsilon)$ (blue), by evolving the system adiabatically along the control loop defined by $\gamma(\varepsilon)$ (orange), and by using an STA (green). The ideal braid and the braid traced by the STA are not necessarily mathematically equivalent, but yield the same swap operation (up to a global phase).

dynamics have been thoroughly experimentally observed in the two-mode case [41–48].

C. Dressed State Approach to Non-Hermitian Shortcuts-to-Adiabaticity

Now that we have laid down the fundamental concepts allowing one to find the correct representation of any non-Hermitian operator in the adiabatic frame, we can formulate a theory to construct non-Hermitian STAs. Our approach builds on the ideology of the dressed state approach for Hermitian systems [27]: If one is only interested in the topological operation generated by encircling an EP with a control loop $\gamma(t) = [\{p_k(t)\}_k]$ of duration $t = t_0$, with $\{p_k\}_k \subseteq \{p_i\}_{i=1}^n$ [see Eq. (1)], then it is not necessary to follow the ideal adiabatic evolution at all times. It is sufficient to generate an evolution that only resembles the adiabatic evolution at a desired final time $t = t_0$ (see Fig. 2). In other words, we ensure only that the end points of the braid strands determined by applying the (non-trivial) STA permutation operation $[\sigma(j), \mathrm{STA}]$ are identical to the braid strands of the ideal (static) eigenvalue braids given by σ [see Eq. (4)]:

$$\begin{aligned} \lambda_{\sigma(j),STA} &= \lambda_{\sigma(j)} \text{ for } t = 0, t_0 \\ \lambda_{\sigma(j),STA} &\not\equiv \lambda_{\sigma(j)} \text{ for } 0 < t < t_0 \end{aligned} \tag{9}$$

Like for Hermitian systems, there are two main ingredients to find non-Hermitian STAs via the dressed-state approach: (1) a choice of dressing transformation $S_{\mathrm{dr,STA}}(t)$ for the instantaneous eigenstates and (2) an associated non-Hermitian control Hamiltonian $W_{\mathrm{STA}}(t)$ such that the modified non-Hermitian Hamiltonian $H_{\mathrm{STA}}(t) = H(t) + W_{\mathrm{STA}}(t)$ generates the desired evolution at $t = t_0$. In addition to these requirements, we must introduce the new constraint that (3) the change of frame operators must be holomorphic functions along $\gamma(t)$, otherwise the non-Hermitian STAs will be unusable. As we show below in Sec. III C 2, and in stark contrast to the Hermitian case, this leads to new versions of known STAs.

The generic dressing transformation given by

$$S_{\mathrm{dr,STA}}[\boldsymbol{p}(t)] = \sum_{j=1}^{n} |\phi_j[\boldsymbol{p}_i(t)]\rangle\langle w_j|, \tag{10}$$

for dressed eigenstates $|\phi_j\rangle$ and dressed frame basis $\{|w\rangle\}_{w=1}^n$, is therefore constructed using the boundary condition

$$S_{\mathrm{dr,STA}}(0) = S_{\mathrm{dr,STA}}(t_0) = \mathbb{1}, \tag{11}$$

which guarantees that the dressed states coincide with the instantaneous eigenstates $|\psi_j\rangle$ at $t = 0, t_0$, satisfying (1). If $S_{\mathrm{dr,STA}}(t) = \mathbb{1}$, then $|\phi_j(t)\rangle = |\psi_j(t)\rangle$ [see Sec. III C 2]. Otherwise the state is allowed to evolve trivially during the loop: $|\phi_j(t)\rangle \not\equiv |\psi_j(t)\rangle$ for $0 < t < t_0$ [see Secs. III C 2 and III C 4].

The dressing operator transforms H_{ad} [see Eq. (8)] into the dressed frame (ignoring time-dependence) according to

$$H_{\mathrm{dr}} = S_{\mathrm{dr,STA}}^{-1} H_{\mathrm{ad}} S_{\mathrm{dr,STA}} - i S_{\mathrm{dr,STA}}^{-1} \dot{S}_{\mathrm{dr,STA}}, \tag{12}$$

where imposing

$$\langle j_{\mathrm{dr}}|H_{\mathrm{dr}}|i_{\mathrm{dr}}\rangle = 0 \tag{13}$$

for all $i_{\mathrm{dr}} \neq j_{\mathrm{dr}}$ allows one to find the control operator W_{STA} that obeys condition (2). This yields the modified dressed Hamiltonian

$$H_{\mathrm{dr,STA}} = H_{\mathrm{dr}} + W_{\mathrm{STA}}, \tag{14}$$

which when transformed back into the original (system) frame,

$$H_{\mathrm{STA}} = H + S_{\mathrm{ad}} S_{\mathrm{dr,STA}} W_{\mathrm{STA}} S_{\mathrm{dr,STA}}^{-1} S_{\mathrm{ad}}^{-1} \tag{15}$$

produces a control field compatible with the constraints of H. Because H_{dr} contains a non-inertial term similar to H_{ad} [see Eq. (8)], any discontinuities incurred in the operator (and/or its derivative) while traversing the parameter loop $\gamma(t)$ would therefore carry over into the construction of W_{STA}, yielding ineffectual control fields. Therefore any prescription for a non-Hermitian STAs must include (3).

In the Hermitian case, any choice of dressing can be viewed as a family of transformations characterized by the loop time t_0 to which there is an associated control operator W_{STA} that generates the STA. In the non-Hermitian case however, this does not hold true; we show in later sections that, for a given $\{p_k\}_k \subseteq \boldsymbol{p}$, constructing a holomorphic dressing operator does not necessarily guarantee a family of solutions, and fails to satisfy Eq. (11) [see Sec. III C 2].

III. EXAMPLE: TWO-MODE SYSTEM

To make things concrete, and without loss of generality, we consider a symmetrized, static two-mode non-Hermitian Hamiltonian that describes two coupled harmonic modes subject to damping [see Fig. 1 (a)]

$$H_{\rm sym} = -\left(\Delta + i\frac{\Gamma}{2}\right)\sigma_z + \Omega\sigma_x. \tag{16}$$

Here, $\Delta = (\omega_1 - \omega_2)/2$, is the frequency detuning, Ω is the coupling strength, and $\Gamma = (\gamma_1 - \gamma_2)/2$ is the difference between the damping rates associated to the individual modes. In spite of its simplicity, Eq. (16) describes several physical platforms [24, 45, 47, 49–52].

The associated eigenvalues are given by

$$\tilde{\lambda}_\pm = \pm\sqrt{\left(\Delta + i\frac{\Gamma}{2}\right)^2 + \Omega^2}, \tag{17}$$

and contain EPs located when $\tilde{\lambda}_\pm = 0$ at $\Delta = 0, \Omega = \pm\Gamma/2$; conversely, the EPs can defined by $f[\boldsymbol{p}] = \left(\Delta + i\frac{\Gamma}{2}\right)^2 + \Omega^2 = 0$ for $\boldsymbol{p} = \{\Delta, \Omega, \Gamma\}$ [see Sec. II A]. Therefore $\tilde{\lambda}_\pm[\gamma(\varepsilon)]$ are discontinuous whenever a closed contour $\gamma(\varepsilon)$ encircles the EP, since it necessarily crosses the branch cut associated with the square root function [see Fig. 3(a)]. Given that the principal square root function has a branch cut along $(-\infty, 0]$ on the real axis, we define the branch cut along

$$\begin{aligned} -\frac{1}{4}\Gamma^2 + \Omega^2 + \Delta^2 \leq 0, \\ \Delta\Gamma = 0, \end{aligned} \tag{18}$$

such that EPs can be consider the end points of the branch cut.

By defining a new domain of definition for the square root function $w(z) = \sqrt{z}$ given by $R \setminus \{l\}$, where $R = \{(z, w) \in \mathbb{C}^2 | w^2 = z\}$ is the Riemann surface associated to the square root function and l is the locus where the eigenvalues are identical, denoting the subspace of EPs, the holomorphic eigenvalues of Eq. (16) can be constructed, given by

$$\lambda_\pm = \cos(\chi)\,\tilde{\lambda}_\pm, \tag{19}$$

where χ is a function that geometrically accounts for the "gluing" of the different leaves of the square root function that make up the Riemann surface [see Fig. 3(b)]. The explicit form of χ is determined based off a given parameterization $\gamma_{\rm circ}(\varepsilon)$, but all parameterizations obey Eq (19) as χ is constructed from the Riemannian manifold associated to the spectrum of $H_{\rm sym}$.

Using [see Eq. (19)] we can write the right eigenvectors in the frame of Eq. (16) such that coefficients in their decomposition are holomorphic functions as desired,

$$|j_{\rm sym}\rangle = \left[-\left(\Delta + i\frac{\Gamma}{2}\right) + \lambda_j\right]|0\rangle + \Omega|1\rangle, \tag{20}$$

for $j \in \{+, -\}$. This immediately yields the change of frame operator that diagonalizes Eq. (16) according to $\tilde{S}_{\rm ad}^{-1} H_{\rm sym} \tilde{S}_{\rm ad}$, and which is holomorphic on $R \setminus \{l\}$, given by

$$S_{\rm ad} = \sum_{j=-,+} |j_{\rm sym}\rangle\langle j_{\rm ad}|, \tag{21}$$

where $|j_{\rm sym}\rangle$ is a left eigenvector expressed in the same frame as Eq. (16) and $|j_{\rm ad}\rangle$ is a right eigenvector expressed in the frame of eigenstates (adiabatic frame).

As an example, let us consider the closed contour $\gamma_{\rm circ}(\varepsilon)$ parameterized by

$$\begin{aligned} \Delta(\varepsilon) &= \Delta_0 \sin(\varepsilon + \varphi), \\ \Omega(\varepsilon) &= \Omega_0 + \Delta_0 \cos(\varepsilon + \varphi), \end{aligned} \tag{22}$$

which describes a circle of radius Δ_0 centered at $(\Delta = 0, \Omega = \Omega_0)$ with φ defining the base point of the contour. Choosing to center $\gamma_{\rm circ}(\varepsilon)$ at the EP located at $(\Delta = 0, \Omega = \Gamma/2)$, we find

$$\chi(\varepsilon) = \pi\Theta\left[\frac{1-d}{2} + \left(\varepsilon - \frac{1}{2} + \frac{\varphi}{2\pi}\right)\right], \tag{23}$$

where $d = \pm 1$ accounts for the orientation of the contour and $\Theta(x)$ is the Heaviside function. Using Eq. (19) we find that $\gamma(\varepsilon)$ leads to a permutation of the eigenvalues such that

$$\lambda_\pm(0) \to -\lambda_\pm(1) = \lambda_\mp(0) \tag{24}$$

for $\varepsilon \in [0, 1]$. This constitutes a continuous eigenvalue braid, shown in Fig. 3(c), and is described by the general eigenvalue permutation $\sigma = \pm 1$ for $j \in \{+, -\}$ [see Eq. (4)]. Along the same contour we have that $|\pm_{\rm lab}(0)\rangle \to |\pm_{\rm lab}(1)\rangle = |\mp_{\rm lab}(0)\rangle$. Thus traversing the contour is analogous to implementing a σ_x operation:

$$\sigma_x|\pm\rangle = |\mp\rangle. \tag{25}$$

which corresponds to the general eigenvector permutation $P = \sigma_x$ [see Eq. (5)].

Finally, we note that for non-Hermitian Hamiltonians with special symmetry like Eq. (16), it is often possible to find the change of frame operator without having to explicitly diagonalize H. Here, by making the analogy to a spin-1/2 in an external magnetic field, where the frame of eigenstates can be found by aligning the quantization axis with the orientation of the spin (rotation of the coordinate system), we find that the change of frame operator can also be written as $\tilde{S}_{\rm ad} = \exp[(-i/2)\tilde{\theta}\sigma_y]$ with the generalized rotation angle given by

$$\tilde{\theta} = -\arctan\left(\frac{\Omega}{\Delta + i\frac{\Gamma}{2}}\right). \tag{26}$$

Considering again the behavior of $\tilde{S}_{\rm ad}$ along a contour $\gamma(\varepsilon)$, we observe that $\tilde{S}_{\rm ad}$ is not continuous with respect

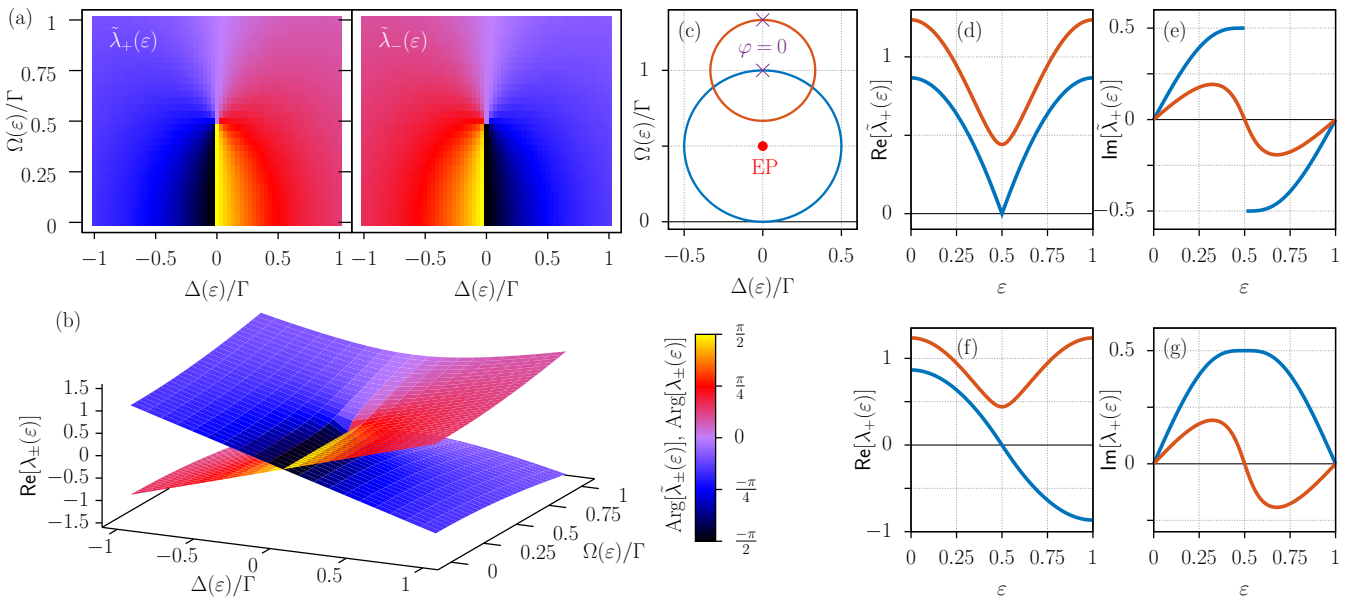

Figure 3. Riemann surface and topology of the square root function. (a) The eigenvalues of a two-mode system correspond to the two branches of the complex square root function. They are discontinuous in the vicinity of an EP, which identifies to the branch point (end of the branch cut) of the square root function. (b) "Gluing" together the branches of the square root functions along the branch cut produces the Riemann surface, where the complex square root function is holomorphic. (c) Example of circular contours [see Eq. (22)] encapsulating (blue) and not encapsulating (orange) an EP. (d) $\mathrm{Re}[\tilde{\lambda}_+]$, (e) $\mathrm{Im}[\tilde{\lambda}_+]$ [see Eq. (17)], (f) $\mathrm{Re}[\lambda_+]$ and (g) $\mathrm{Im}[\lambda_+]$ Eq. (19)] color-coded based on the two loops defined in (c). A contour not encapsulating the EP does not cross the branch cut. The blue contour in (c) is parameterized by $\Delta_0 = \Omega_0 = \Gamma/2, \varphi = 0, d = 1, \Gamma = 1$ (which, if otherwise stated, are the default parameters used in the results), and the orange contour by $\Delta_0 = \Gamma/4, \Omega_0 = \Gamma, \varphi = 0, d = 1, \Gamma = 1$.

to ε when the branch cut associated to the arctan function defining $\tilde{\theta}$ is crossed; $\arctan(z)$ has branch cuts along $(-i\infty, -i] \cup [i, i\infty)$ on the imaginary axis. Like previously, we can define a new domain of definition for the arctan function that corresponds to its Riemann surface with the location of the EPs removed, which yields the holomorphic generalized rotation angle

$$\theta = -\arctan\left(\frac{\Omega}{\Delta + i\frac{\Gamma}{2}}\right) + \chi, \tag{27}$$

with χ the same function as the one introduced in Eq. (19). This yields the desired holomorphic change of frame operator

$$S_{\mathrm{ad}} = \exp\left[-\frac{i}{2}\theta\sigma_y\right], \tag{28}$$

and associated eigenvectors with holomorphic coefficients. Performing the similarity transformation, one obtains

$$H_{\mathrm{diag}} = S_{\mathrm{ad}}^{-1} H_{\mathrm{sym}} S_{\mathrm{ad}} = \lambda_\pm \sigma_{z,\mathrm{diag}}. \tag{29}$$

with $\lambda_\pm$ given by Eq. (19), which immediately yields the holomorphic eigenvalues.

A. Non-Hermitian Systems and Violation of the Adiabatic Theorem

In order to get a heuristic picture of the failure of the adiabatic condition, we consider the dynamic, two-mode non-Hermitian Hamiltonian where $H_{\mathrm{sym}}(\varepsilon) \to H_{\mathrm{sym}}(t)$ for $t \in [0, t_0]$, where t_0 is the characteristic time needed to perform the control loop. Here $\Delta[\varepsilon(t)]$ and $\Omega[\varepsilon(t)]$ are parameterized according to Eq. (22) and we choose

$$\varepsilon(t) = d\left[6\left(\frac{t}{t_0}\right)^5 - 15\left(\frac{t}{t_0}\right)^4 + 10\left(\frac{t}{t_0}\right)^3\right], \tag{30}$$

to be a smooth function of time, i.e., $\dot{\varepsilon}(0) = \dot{\varepsilon}(t_0) = \ddot{\varepsilon}(0) = \ddot{\varepsilon}(t_0) = 0$ (where $\ddot{x} = \mathrm{d}^2x/\mathrm{d}t^2$), and d accounts the loop orientation (± 1 for clockwise/counter-clockwise).

By transforming H_{sym} [see Eq. (16)] into the frame of instantaneous eigenstates using $S_{\mathrm{ad}}(t)$ [see Eq. (28)] we find

$$H_{\mathrm{ad}}(t) = \lambda(t)\sigma_{z,\mathrm{ad}} - \frac{1}{2}\dot{\theta}(t)\sigma_{y,\mathrm{ad}} \tag{31}$$

To observe the failure of the adiabatic theorem, we plot the transition probabilities of the eigenvectors [see Eq. (20)] using

$$P_{i,j}(t) = \frac{|\Phi_{i,j}(t)|^2}{\sum_i^j |\Phi_{i,j}(t)|^2}, \tag{32}$$

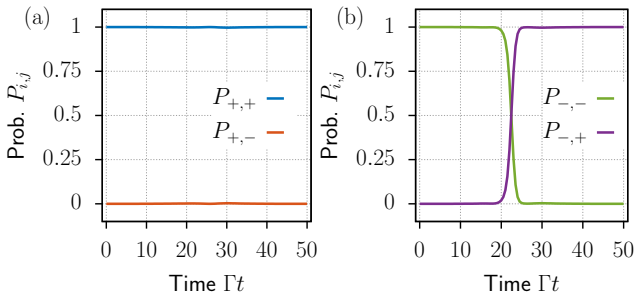

Figure 4. Non-reciprocal dynamics with a two-mode system. Implementing a clockwise control loop around an EP leads to (a) $P_{+,+}(t_0) = 1, P_{-,+} = 0$ and (b) $P_{+,-}(t_0) = 1, P_{-,-}(t_0) = 0$. We use $\Gamma t_0 = 50$.

for $i, j \in \{+, -\}$, and the adiabatic flow matrix Φ_{ad} [see Eq. (6)]. In Fig. 4 we recover the expected results; namely, we see that $P_{+,+}(t) = 1$ for all times, meaning the gain mode is adiabatically evolving, and λ_+ [see Eq. (19)] is tracing its expected braid along the contour defined by Eq. (22). Likewise, $P_{-,-}(t) = 0$ indicates that (almost) all of the initial amplitude in the loss mode has been transferred to the gain mode (despite being in the adiabatic limit), and so λ_- fails to trace its expected braid.

This model has been extensively studied [], but we mention it once more to clearly state the base outcome for which we will compare our STAs against. These STAs will provide various methods to ensure that $P_{-,+}(t_0) = 0$ and $P_{-,-}(t_0) = 1$, mimicking adiabaticity for the loss mode and ensuring eigenvalue braiding.

B. Near Ideal Permutation Operation via Near-Coherent Evolution

Since the topology of the Riemann surface is different than the topology of the parameter space, choosing different base points φ along the same contour encapsulating an EP will result in different eigenvalue braids. Among the infinity of braids associated to the same contour with different φ, there is one braid that can be traced by evolving the non-Hermitian operator H_{sym} describing the dynamics. This braid is associated to a non-Hermitian operator whose imaginary part of the spectrum is anti-symmetric with respect to $t_0/2$ (all the imaginary parts of all of the eigenvalues have to be anti-symmetric), as shown in Fig. 5(a). For this special case there is on average (by the end of the loop, at $t = t_0$) no gain/loss.

So far for the choice of contour given in Eq. (22), which encircles and is centered at an EP, we have considered a base point located at $\Delta = 0, \Omega = \Omega_0 + \Delta_0$, i.e., $\varphi = 0$. Assuming the contour is centered at the EP, by setting the base point at $\Delta = 0, \Omega = \Omega_0 - \Delta_0$, i.e., $\varphi = \pi$, $\text{Im}[\lambda_\pm(\varepsilon)]$ becomes anti-symmetric with respect to $t = t_0/2$.

As a consequence, the flow matrix Φ [see Eq. (6)] produces "quasi"-unitary dynamics when observing the transition probabilities $P_{i,j}$ [see Eq. (32)] at the final loop time $t = t_0$. We show this behavior in Fig. 5(b) where we plot $P_{i,j}(t_0)$ for $i \neq j$ and $i, j \in \{+, -\}$ and find specific loop times Γt_0 where the mode-switching transitions are nearly 0, and thus the ideal adiabatic dynamics are nearly produced.

The difficulty lies in realizing these special loop times with the necessary precision to obtain the desired destructive interference. In Fig. 5(b) we plot the final transition probabilities $P_{i,j}(t_0)$ for the two-mode case over a range of loop times for the non-adiabatic transitions and see distinct times for which $P_{+,-}(t_0) = P_{-,+}(t_0) = 0$, which again generate the same result as the ideal adiabatic dynamics.

However high precision is necessary to achieve these times which is challenging for conventional experimental systems; the results in Fig. 5(b) suggest very narrow dips in time, and any imprecision in timing will result in imperfect destructive interference while tracing a braid different than the one generate by adiabatic dynamics. In Figs. 5(c) and (d) we plot all the transitions probabilities at one of these critical times and show the near ideal adiabatic evolutions of the gain $P_{+,+} = 1$ and loss $P_{-,-} = 1$ modes. Clearly the evolution is not adiabatic at all times and so the braid traced must be different than the ideal braid, but the end result is the same.

As we show in Sec. III B, choosing a base point such that the $\text{Im}[\lambda_\pm]$ [see Eq. (19)] is anti-symmetric with respect to $t = t_0/2$ will help us reduce the overall cost of STA protocols.

This has been previously reported by Arkhipov et al. [53], however, an intuitive physical explanation is lacking and the authors do not comment on the fact that it only works for special times, that $\text{Im}[\lambda_\pm]$ must be anti-symmetric, and that any experimental imprecision may lead to a corrupted dynamics.

C. Non-Hermitian STAs

- Delete any "general" statement. This is now only for the two-mode as an example.
- The main section should now be "Example: Two-mode system". This should become a subsection of that.

1. *Transitionless Driving*

We start by considering the non-Hermitian equivalent of the well-known STA coined Transitionless Driving (TD) [54, 55]. The dressing transformation leading to TD is the trivial dressing

$$S_{\text{dr,TD}}(t) = \mathbb{1}, \tag{33}$$

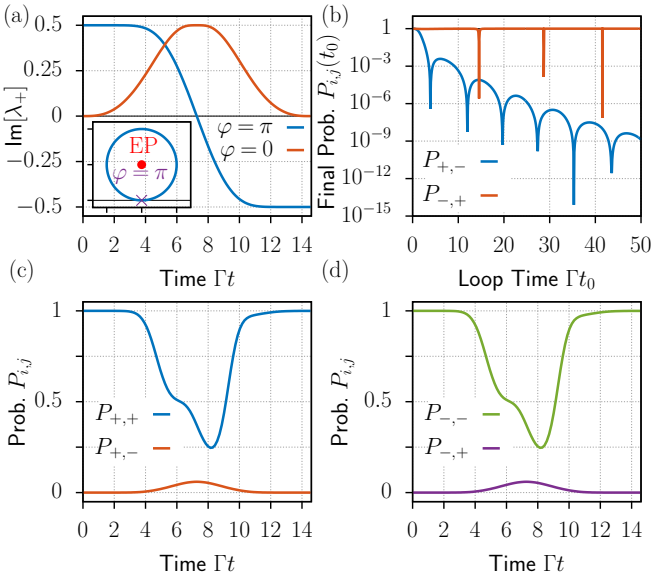

Figure 5. Dynamics using $\varphi = \pi$. (a) $\mathrm{Im}[\lambda_+(t)]$ using blue contour shown in Fig. 3(d). (b) Non-adiabatic transition probabilities $P_{i,j}$ [see Eq. (32)] at $t = \Gamma t_0$. At $\Gamma t_0 \approx 14.5$, we plot the transition probabilities, given in (c) and (d). The remaining parameters are given the default values (see Fig. 4).

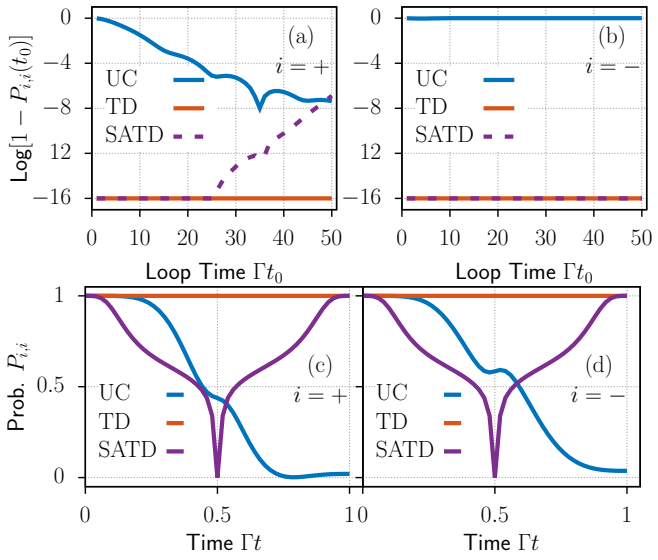

Figure 6. Transition probabilities, $P_{i,j}(t)$ [see Eq. (32)]. Final probability error $\mathrm{Log}[1 - P_{i,i}(t = \Gamma t_0)]$ for (a) $i = +$ and (b) $i = -$ for range of loop times Γt_0. The results are valid up to 10^{-16}, which is the limit of the numerical precision for the solver used. TD [see Secs. III C 2 and SATD [see Sec. III C 2] always yield a braid associated to $H_{\mathrm{sym,STA}}$ that matches the ideal braid of H_{sym} by the end of the loop. $P_{i,i}(t)$ using $\Gamma t_0 = 1$ using (c) $i = +$ and (d) $i = -$. TD traces the ideal braid at all times, while SATD guarantees that the final result is identical to the ideal case. The tested parameter values in (a) and (b) are the default parameters [see Fig. 3] with $\Gamma t_0 = 1$, and for (c) and (d) $\Delta_0 = \frac{1}{2}, \Omega_0 = \frac{1}{6}, \varphi = -\frac{\pi}{8}, d = 1, \Gamma t_0 = 2, \Gamma = 1$.

which guarantees that the dressed states ϕ_j [see Eq. (10)] correspond at all times to the instantaneous eigenstates of H_{sym} ϕ_j [see Eq. (7)]. We find the (naive) TD control operator, which in the frame of instantaneous eigenstates (adiabatic frame) of $H_{\mathrm{sym}}(t)$ takes the form

$$\tilde{W}_{\mathrm{TD}} = +i\tilde{S}_{\mathrm{ad}}^{-1}\dot{\tilde{S}}_{\mathrm{ad}} = \frac{1}{2}\dot{\tilde{\theta}}\sigma_{\mathrm{y,ad}}, \tag{34}$$

where we drop the "ad" subscript when referring to STA corrections in the adiabatic frame. This completely suppresses all non-adiabatic transitions by eliminating the non-inertial term in Eq. (31). Expressing Eq. (34) in the same frame as H_{sym}, we find

$$\tilde{W}_{\mathrm{sym,TD}} = \tilde{S}_{\mathrm{ad}}\left(\tilde{W}_{\mathrm{TD}}\right)\tilde{S}_{\mathrm{ad}}^{-1} = \frac{1}{2}\dot{\tilde{\theta}}\sigma_{\mathrm{y}}. \tag{35}$$

We emphasize once more the importance of satisfying condition (3) [see Sec. II C] by defining change of frame operators that are holomorphic to obtain well-behaved control operators; Eqs. (34) and (35) depend explicitly on the derivative of $\tilde{S}_{\mathrm{ad}}$. By substituting Eq. (28) into Eq. (34) we find the holomorphic control operator

$$W_{\mathrm{TD}} = \frac{1}{2}\dot{\theta}\sigma_{\mathrm{y,ad}}. \tag{36}$$

For the example considered here, regardless if we use the non-holomorphic $\tilde{S}_{\mathrm{ad}}$ or the holomorphic S_{ad}, we will yield the same W_{TD} in the lab frame. This follows from having $\dot{\tilde{\theta}} = \dot{\theta}$ up to a constant, and $[\tilde{S}_{\mathrm{ad}}, \sigma_y] = [S_{\mathrm{ad}}, \sigma_y]$ =0. We stress, however, that this is unique to the to the two-mode non-Hermitian Hamiltonian [see Eq. (16)] considered here and in general constructing $\tilde{W}_{\mathrm{TD}}$ from $\tilde{S}_{\mathrm{ad}}$ will result in in a discontinuous control operator that does not generate the desired dynamics.

$H_{\mathrm{sym,TD}} = H_{\mathrm{sym}} + W_{\mathrm{sym,TD}}$ restores the permutation of eigenvectors according to σ_x [see Eq. (25)], and ensures the adiabatic and dressed states are always identical. We plot this in Figs. 6(a) and 6(b), where we show the error of the final transition probabilities $\mathrm{Log}[1 - P_{i,i}]$ for $i \in \{+, -\}$ respectively [see Eq. (32)], obtained for the circular path [see Eq. (22)] over a range of loop times Γt_0. We see that TD behaves as in the Hermitian case and one can view W_{TD} as a family of corrections labelled by the parameter t_0 since the error is less than the limit of the numerical precision of the solver used $-16 > \mathrm{Log}[1 - P_{i,i}]$. As we discuss below, and in contrast to the Hermitian case, this is in general not true for non-Hermitian systems.

Additionally, we plot the transition probabilities $P_{i,i}$ in Figs. 6(c) and 6(d) for $i \in \{+, -\}$ respectively, for the same circular path and a given loop time $\Gamma t_0 = 1$. As expected, $H_{\mathrm{sym,TD}}$ generates a dynamics that mimics the ideal adiabatic dynamics of H_{sym}.

To demonstrate that TD only emulates the adiabatic

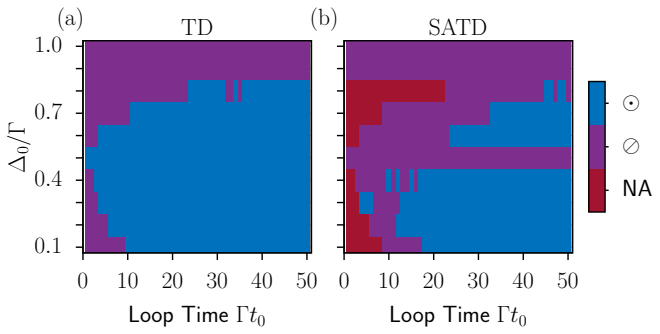

Figure 7. Exceptional point encircling check [see Eq. (37)] for (a) TD correction [see Sec. III C 2] and (b) SATD correction [see Sec. III C 2]. We find that TD and SATD ensure eigenvalue braiding for all (applicable) parameter sets, but the EP associated to $H_{\text{sym,STA}}$ is not necessarily encircled. The labeling scheme is as follows: ⊙ - EP encircled, ⊘ - EP not encircled, NA - not applicable. Braiding of the eigenvalues associated to $H_{\text{sym,mod}}$ [see Eq. (38)]is observed for all (applicable) parameter sets.

dynamics around an EP, we verify that there exists values of t_0 for which the control loop does not encapsulate an EP associated to the spectrum of $H_{\text{sym,mod}}$. For traceless operators the following conditions can be used to determine if there is an eigenvalue braid:

$$\begin{aligned} &\text{I}: \lambda_{\pm,\text{STA}}(0) = -\lambda_{\pm,\text{STA}}(t_0) = \lambda_{\pm,\text{STA}}(2t_0), \\ &\text{II}: \int_0^{t_0} \lambda_{\pm,\text{STA}} \mathrm{d}t \neq 0 \; ; \; \int_0^{2t_0} \lambda_{\pm,\text{STA}} \mathrm{d}t = 0. \end{aligned} \tag{37}$$

where

$$\lambda_{\pm,\text{STA}} = \pm \cos(\chi_{\text{STA}}) \sqrt{\left(\Delta + i\frac{\Gamma}{2}\right)^2 + \Omega^2 + W^2_{\text{sym,STA}}} \; , \tag{38}$$

uses $\chi_{\text{STA}}(t)$ [see Eq. (23)] for the new manifold determined from $H_{\text{sym,STA}}$. If the operator is not traceless, then one must add to relations (I) and (II), on both sides of the equality, the value of the trace.

For 2-strands braid, concatenating two non-trivial braid leads to the identify braid; going once around EP generates a braid, and going a second time around the EP generates the inverse braid. The contour resulting by concatenating twice $\gamma[\varepsilon(t)]$ yields eigenvalues $\lambda_{\pm}(t)$ that are asymmetric with respect to t_0. This implies that an EP is encircled when condition (II) in Eq. (37) is met.

In Fig 7(a) we check the "encircling-an-EP" criterion (II) [see Eq. (37)] for TD using $\lambda_{\pm,\text{TD}}$ over a range of loop times $\Gamma t_0 \in [0.1, 50]$ and radii $\Delta_0/\Gamma \in [0.1, 1]$. It is sufficient only to check criterion (II) since $\lambda_{\pm,\text{STA}}$ always satisfies criterion (I) by construction ($\lambda_{\pm,\text{TD}}$ traces the ideal braid). Therefore, as expected, we find that $H_{\text{sym,TD}}$ always yields an eigenvalue braid without necessarily encircling an EP associated to the spectrum of $H_{\text{sym,TD}}$.

In Sec. III B we showed that there are combinations of contours and base points that can result in control loops that generate coherent dynamics. By fine tuning the loop time t_0, destructive interference will lead to $P_{i,i} = 1$ and $P_{i,j} = 0$ $(i \neq j)$, for $i, j \in \{+, -\}$. It is only natural to ask if, in such a scenario, the TD correction yields modified control fields with a smaller amplitude. We can compare amplitudes of different prescriptions by finding the root mean square (RMS) amplitude: For an operator given by $H = a(t)\sigma_x + b(t)\sigma_y + c(t)\sigma_z$, with a, b, $c \in C$, the RMS amplitude is given by

$$\text{RMS} = \frac{1}{t_0} \int_0^{t_0} \sqrt{|a(t)|^2 + |b(t)|^2 + |c(t)|^2} \; \mathrm{dt}. \tag{39}$$

In Fig. 8(a), we plot the RMS amplitudes for the uncorrected (UC) and TD case obtained for the circular path centered at the EP for $\varphi = 0$ and $\varphi = \pi$ [see Eq. (22)]. Using $\varphi = \pi$ reduces the overall "cost" of implementing the TD correction. In Figs. 8(b) and 8(c) we plot the real and imaginary parts of W_{TD} for $\varphi = 0$ and $\varphi = \pi$. The latter case generates a dynamics for which destructive interference is possible. We find that there is no significant difference in the field amplitude between $\phi = 0$ and $\varphi = \pi$.

This is to be expected since TD must "work hard" to generate a dynamics that mimics at all times the ideal adiabatic dynamics of H_{sym}. TD can therefore not benefit from the coherent dynamics happening at special values of Γt_0 and $\phi = \pi$, and can *only mimic* the ideal dynamics at the initial and final times. As we discuss below, this is in stark contrast to other control operators found with non-trivial dressings and which greatly take advantage (in term of resources) of correcting a dynamics which partly produces the desired result.

2. *Super Adiabatic Transitionless Driving*

Despite its effectiveness, the TD correction may be considered to demanding, as it often requires resources incompatible with the original physical systems [56], e.g., for the two-mode model considered one must be able to couple to σ_y. To overcome this limitation, an STA coined superadiabatic transitionless driving (SATD) was introduced [27, 57]. SATD is known to yield correction fields that are compatible with the constraints of a two-level system and a lambda system [27, 58].

Fundamentally, SATD is a special case of the dressed state approach to STAs in which the dressing is chosen to diagonalize the adiabatic Hamiltonian (which includes the non-inertial term that couples the instantaneous eigenstates [see Eq. (31)]).

For Hermitian systems, independently of the protocol time t_0, SATD always yields a modified Hamiltonian $H_{\text{sym,SATD}}$ that generates a dynamics that allows one to evolve $|\psi_i(0)\rangle$ to $|\psi_i(t_0)\rangle$ without the system occupying $|\psi_i(t)\rangle$ with unit probability at intermediate times. For non-Hermitian systems, however, this is not the case and SATD cannot be viewed as a family of solutions labelled by the protocol time t_0.

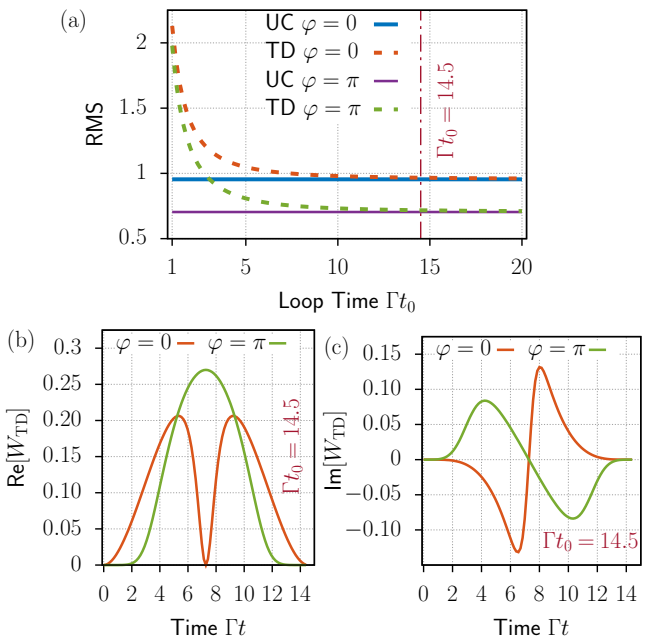

Figure 8. (a) Comparison of RMS [see Eq. (39)] amplitudes. Example of (b) real and (c) imaginary parts of TD correction W_{TD} for $\Gamma t_0 = 14.5$. Leveraging the quasi-coherent regime of the uncorrected dynamics does yield TD fields with reduced amplitude (see main text for more details).

For the two-mode system described by Eq. (16) we have

$$\tilde{S}_{\mathrm{dr,SATD}} = \exp\left[-\frac{i}{2}\tilde{\mu}\sigma_x\right], \tag{40}$$

using the generic dressing angle $\tilde{\mu}$ that satisfies Eq. (11). For the valid dressing angles, the non-Hermitian control Hamiltonian is given by:

$$\begin{aligned} &H_{\mathrm{sym,SATD}} \\ &= S_{\mathrm{ad}} S_{\mathrm{dr,SATD}} \left(H_{\mathrm{dr,SATD}}\right) S^{-1}_{\mathrm{dr,SATD}} S^{-1}_{\mathrm{ad}} \\ &= H_{\mathrm{sym}} + g_x\sigma_x + g_z\sigma_z \end{aligned} \tag{41}$$

SATD is a specific dressing that uses a $\tilde{\mu}$ that diagonalizes H_{ad}

$$\tilde{\mu} = -\arctan\left[\frac{\frac{1}{2}\dot{\theta}}{\lambda_\pm}\right]. \tag{42}$$

where $\lambda_\pm$ and θ are given by Eq. (19) and Eq. (27), respectively. This yields an SATD dressing angle that has boundaries properties that are fundamentally different than its counterpart defined in Eq. (27): Since $\lim_{t\to 0,t_0} \dot{\theta}(t)/\lambda_\pm(t) \to 0$, we have $\tilde{\mu}(0) = \tilde{\mu}(t_0) = 0$ that yields $\tilde{S}_{\mathrm{dr,SATD}}(0) = \tilde{S}_{\mathrm{dr,SATD}}(t_0) = \mathbb{1}$ as required by Eq. (11) [see Sec. II C].

Similarly to the generalized rotation angle defining S_{ad} [see Eq. (28)], $\tilde{\mu}$ is not holomorphic since arctan has a branch cut along the imaginary axis [see Sec. III]. To correctly define the change of frame, we must first define $\tilde{\mu}$ on its associated Riemann surface. Similar for θ, this implies finding the function χ_{SATD} that geometrically accounts for the "gluing" of the leaves of the arctan function which yields the holomorphic function μ. For a two-mode system, as discussed above, this is done by adding a phase shift of $\pm\pi$ to $\tilde{\mu}$ each time the branch cut of arctan is crossed such that

$$\mu = \tilde{\mu} + \chi_{\mathrm{SATD}}. \tag{43}$$

Assuming that a choice of contour in parameter space results in $\mu(t_0) = \tilde{\mu}(t_0) + n\pi = n\pi$, with n an integer, then

$$S_{\mathrm{dr}}(t_0) = \exp\left[\pm\frac{i}{2}(n\pi)\sigma_x\right] = (-i)^n\sigma_x^n. \tag{44}$$

If n is an even integer then, Eq. (44) reduces to $(-i)^n\mathbb{1}$ and Eq. (11) of the dressed state approach [see Sec. II C] is fulfilled up to an (irrelevant) global phase, and can be used to build the SATD correction

$$W_{\mathrm{SATD}} = +iS^{-1}_{\mathrm{dr,SATD}}\dot{S}_{\mathrm{dr,SATD}} = \frac{1}{2}\dot{\mu}\sigma_x, \tag{45}$$

and the correction fields

$$\begin{aligned} g_x &= \frac{\cos\theta}{2}\left[-\frac{\dot{\theta}\dot{\lambda} - \lambda\ddot{\theta}}{\lambda^2 + \dot{\theta}^2}\right], \\ g_z &= -\frac{\sin\theta}{2}\left[-\frac{\dot{\theta}\dot{\lambda} - \lambda\ddot{\theta}}{\lambda^2 + \dot{\theta}^2}\right]. \end{aligned} \tag{46}$$

However, if n is an odd integer, then Eq. (44) reduces to $(-i)^n\sigma_x$, which violates Eq. (11) and immediately shows that SATD is not a valid STA.

This discussion is in contrast to Sec. III C 2, where we stressed that for the two-mode example considered here using the *inappropriate* change of frame $\tilde{S}_{\mathrm{ad}}$ [see Eq. (21)] would yield, due to mathematical properties, the same control operator $W_{\mathrm{sym,TD}}$ as the one predicted by the correct (holomorphic) change of frame S_{ad} [see Eq. (28)]. For any other dressing, including SATD, using $\tilde{S}_{\mathrm{ad}}$ to express the control operator in the lab frame will result either in the wrong predictions for g_x and g_z or discontinuous fields.

We illustrate this behavior in Fig. 9(a) where we plot $\mu(t_0)$ as a function of t_0 for the for two different circular contours Eq. (22). The dressing angle along the first contour always defines a valid SATD dressing, while along the second contour there are loop-time intervals for which SATD is not an appropriate dressing. In general, for a given choice of contour, SATD will fail for shorter loop times [see Fig. 9(a)]. This follows from $\dot{\theta}(t)$ scaling like $1/t_0$ which can result in the imaginary part of the argument of Eq. (43) becoming larger (smaller) than +1 (-1).

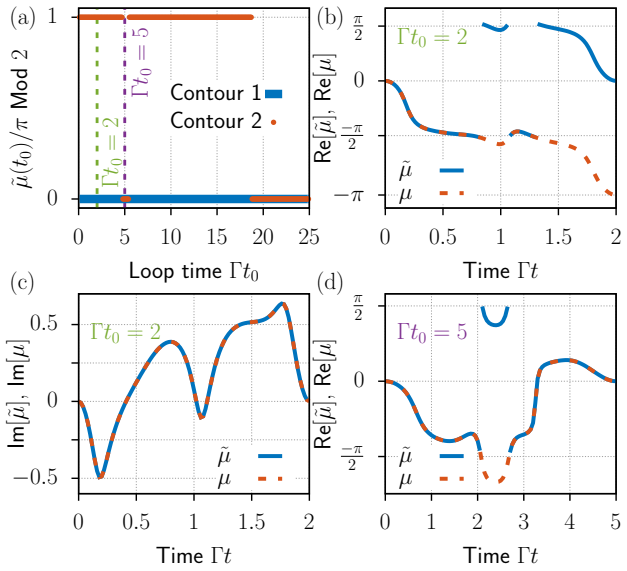

Figure 9. Determining the validity of SATD. (a) SATD is not a valid STA over the whole range $\Gamma t_0 = [0, 25]$ for contour 2 (circular contour with $\Delta_0 = \frac{1}{2}, \Omega_0 = \frac{1}{6}, \varphi = -\frac{\pi}{8}, d = 1, \Gamma = 1$) while it is a valid STA for contour 1 over the same range Γt_0. Example of SATD dressing angles plotted using (b), (c) an invalid SATD $[\tilde{\mu}(t_0) = 0 \neq (\mu(t_0)/\pi)\text{Mod}2]$ and (c) a valid SATD $[\tilde{\mu}(t_0) = 0 = (\mu(t_0)/\pi)\text{Mod}2]$.

In Figs. 9(b)-Fig. 9(d) we show examples [corresponding to loop times marked by a green and purple line in Fig. 9(a)], where defining Eq. (43) on its associated Riemann surface produces a dressing that violates [Fig. 9(b) and 9(c)] and fulfills [Fig. 9(d)] the boundary condition for the dressing transformation [see Eq. (11)]. We stress that this behavior is generic for any finite dimension and dressing choice, and is not specific to either the two-mode system we consider or SATD.

When using a valid dressing angle, the dynamics produced are as expected according to Eq.(9): the braid traced is not identical to the ideal adiabatic braid, but the end points are equivalent. We show this in Figs. 6(a) and 6(b) by plotting the error of the final transition probabilities $\text{Log}[1-P_{i,i}]$ for $i \in \{+,-\}$ respectively [see Eq. (32)] when using the circular parameter loop parameterized by Eq. (22) over a range of loop times Γt_0. SATD almost always exceeds the numerical precision of the solver.

In Figs. 6(c) and 6(d) we plot the transition probabilities $P_{i,i}$ for $i \in \{+,-\}$ respectively for the same path and a given loop time $\Gamma t_0 = 1$. As expected $H_{\text{sym,SATD}}$ only ensures the initial and final times of the dynamics correspond to the ideal adiabatic dynamics, allowing the intermediate times to evolve trivially.

Similar to our analysis of the TD correction in Sec.III C 2, we check that the braids generated by $H_{\text{sym,SATD}}$ are not linked to encircling an EP belonging to the spectrum of $H_{\text{sym,SATD}}$. We plot this in Fig. 7(b) and find the same result as TD, namely $H_{\text{sym,SATD}}$ always produces a braid regardless of encircling the EP associated to the spectrum of $H_{\text{sym,SATD}}$, provided the chosen dressing angle satisfies Eq. (11).

In Sec. III B, we discussed that there exists choices of base points for a same contour that can lead to the the imaginary part of the spectrum to be anti symmetric with respect to $t = t_0/2$. Evolving the system along the associated control loop and fine-tuning the duration of the loop t_0, one can generate a coherent dynamics that leads to $P_{i,i}(t_0) = 1$ for $i \in \{+,-\}$ [see Fig. 5], but with $P_{i,i}(t_0) \neq 1$ for intermediate times.

In Fig. 10(a) we compare the SATD field amplitudes with the uncorrected fields (UC) using the RMS [see Eq. (39)] amplitude, for a circular path of radius Δ, centered at $\Delta_0 = 0, \Omega_0 = 0.5$, and different base-points parameterized by $\varphi = 0$ and $\varphi = \pi$. On average the SATD fields benefit from the quasi-coherent regime choice, verifying if we can reduce the resources needed to implement the control field.

For one of the times which allow one to generate a quasi-coherent dynamics that yield the same result at $t = t_0$ as adiabatic passage, we plot we plot the real and imaginary parts of the SATD control field g_x [see Eq. (46)] in Figs. 10(b) and (c) and contrast them for $\varphi = 0$. We find this chose reduces the field amplitudes by more than 50%. This is expected because SATD benefits from the quasi-coherent regime since using $\varphi = \pi$ steers the uncorrected system H_{sym} closer to the desired dynamics, reducing the amplitude of the SATD fields, which are sensitive to the deviations away from the adiabatic dynamics.

3. *Robustness Analysis*

It has been shown for Hermitian systems that STAs inherit some of the robustness of the adiabatic protocol it originates from [23]. In the case of imprecisions due to parameter uncertainties, robustness is guaranteed as long as the characteristic magnitude of the uncertainties is smaller than the smallest gap between instantaneous eigenstates.

For non-Hermitian systems, however, parameter uncertainties can result in complete failure of the STA. This phenomenon is analogous to the violation of the adiabatic theorem for non-Hermitian systems: parameter uncertainties lead to transitions between instantaneous eigenstates which can be amplified in non-Hermitian systems [see Sec. III C 3].

We show this behavior for the two-mode system we considered throughout. Choosing again the circular contour defined in Eq. (22), we assume an uncertainty in the radius given by $\delta\Delta_0$ and characterized by a normal Gaussian distribution

$$p(\delta\Delta_0) = \frac{1}{\beta\sqrt{2\pi}} \exp\left[-\frac{1}{2}\left(\frac{x}{\beta}\right)^2\right], \qquad (47)$$

with mean 0 and standard deviation β. Such an uncertainty can, e.g., originate from an amplitude uncertainty

[VC 7] im not sure thi EQ makes sense, why the p()?

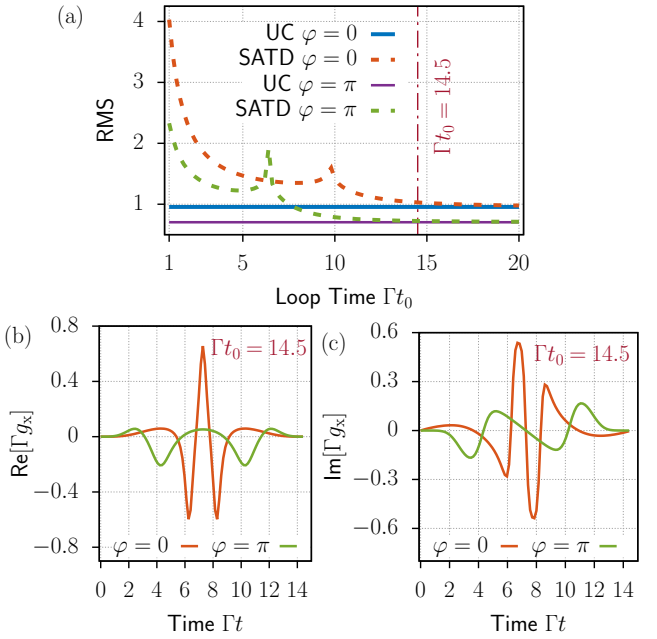

Figure 10. (a) Comparison of RMS [see Eq. (39)] amplitudes. Example of real (b) and (c) imaginary parts SATD correction field g_x [see Eq. (46)] comparing $\varphi = 0$ and $\varphi = \pi$ for $\Gamma t_0 = 14.5$. The correction amplitudes are significantly reduced in the quasi-coherent regime.

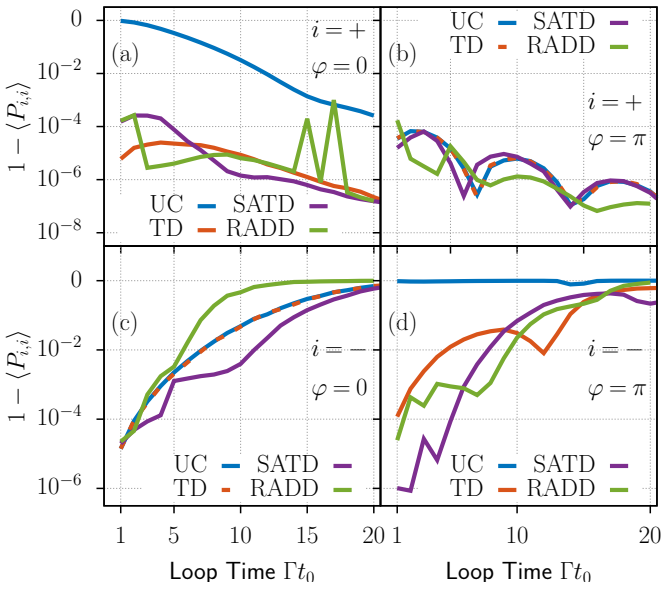

Figure 11. Robustness of STAs against parameter variations. (a) Average fidelity error $1 - < P_{+,+} > (t_0)$ as a function of $\Gamma t_0$for a circular control loop using $\varphi = 0$. (b) Same as (a) but with $\varphi = \pi$. (c) Same as (a) for $1 - < P_{-,-} > (t_0)$. (d) Same as (c) for $\varphi = \pi$.

in the control fields used to drive the physical system.

To understand how uncertainties lead to a complete failure of the STA, it is useful to express $H_{\rm sym,imp} = H_{\rm sym} + \delta\Delta_0\sigma_z$ in the frame of instantaneous eigenstates of $H_{\rm sym}$. Using the change of frame operator given in Eq. (28), we get

$$H_{\rm ad,imp}(t) = H_{\rm ad}(t) + \delta\Delta_0(t)\big[\cos(2\theta)\,\sigma_z - \sin(2\theta)\,\sigma_x\big], \tag{48}$$

with $H_{\rm ad}$ given in Eq. (31).

Equation (48) shows that imprecisions that couple to σ_z in lab frame yield non-adiabatic transitions in the frame of instantaneous eigenstates. STAs cannot average out the effects of this non-adiabatic term since the value of $\delta\Delta_0$ is unknown.

VC 8] also his one, i ont think his is liter- lly what we lot

We plot in Fig. 11 the average fidelity error

$$\langle P_i, j\rangle = \int_{-\infty}^{\infty} {\rm d}\delta\Delta_0\ {\rm p}(\delta\Delta_0)\langle i|\Phi_{\rm ad,imp}(t_0)|j\rangle^2, \tag{49}$$

where $\Phi_{\rm ad,imp}$ [see Eq. (6)] is the flow matrix determined using Eq. (48)as a function of the loop time t_0 for both $\varphi = 0$ and $\varphi = \pi$ [see Eq. (32)]. We recall that the control loop associated to a circular path centered at the EP [see Eq. (22)] parameterized by $\varphi = \pi$ gives rise to quasi-unitary dynamics.

Our results show that in the long loop-time limit ($\Gamma t_0 \gg 1$) STAs cannot mimic adiabatic dynamics, since the imprecisions yield non-adiabatic transitions that undergo amplification, as expected. However, in the short loop-time limit, since there is not enough time to amplify non-adiabatic transitions, STAs present some robustness against parameter uncertainties. For a loop time $\Gamma t_0 \lesssim 5$, we find a state fidelity error $[1 - \langle P_{-,-}\rangle] < 10^{-2}$.

In principle, the non-Hermitian versions of TD and SATD would allow one to realize eigenvalue braiding in an experimental setup, even in the presence of uncertainties, given that one performs a "fast" control loop. However, this implies the ability to realize control fields with relatively large amplitudes since the corrections fields scale like $1/t_0$.

In the next section, we show how an appropriate choice of dressing leads to control fields with a moderate amplitude even in the short loop-time limit. This type of STA has the advantage to require less resources and can, thus, be easier to implement in a given experimental platform.

4. *Reduced Amplitude Dressed Driving*

We design a dressing that yields control fields with amplitudes smaller than TD and SATD. To this end, we consider a modification of the SATD dressing angle given by

$$\mu_{\rm mod}(t) = -\arctan\left[\frac{\frac{1}{2}\dot\theta(t)}{\lambda(t)[1 + {\rm F}(t)]}\right], \tag{50}$$

where

$$\mathrm{F}(t) = \mathrm{A}\exp\left[\left(\frac{t - t_0/2}{\beta}\right)^{2n}\right], \tag{51}$$

is a a hyper-Gaussian mask function with free parameters A, β, and n. The purpose of $F(t)$ is to reduce the overall amplitude of $g_{x,\mathrm{mod}}$ and $g_{z,\mathrm{mod}}$ which are related to the amplitude of μ_{mod} and its first derivative.

$$\begin{aligned} g_{z,\mathrm{mod}} &= -\frac{i\Gamma}{2} - \Delta + \frac{1}{2}\dot{\theta}\cot\mu_{\mathrm{mod}}\sin\theta + \frac{\dot{\mu}_{\mathrm{mod}}}{2}\cos\theta, \\ g_{x,\mathrm{mod}} &= -\Omega - \frac{1}{2}\dot{\theta}\cot\mu_{\mathrm{mod}}\cos\theta + \frac{\dot{\mu}_{\mathrm{mod}}}{2}\sin\theta. \end{aligned} \tag{52}$$

To minimize the amplitude of $g_{x,\mathrm{mod}}$ and $g_{z,\mathrm{mod}}$ we look for the set of values $\{A, \beta, n\}$ that minimize the RMS amplitude [see Eq. (39)] of the control fields for a given t_0. The minimization procedure is done by considering values of A to the interval $[10^{-2}, 10]$, the values of n to be integers between 1 and 7, and the values β to the interval $[t_0/25, t_0/3]$. This defines a new STA which we coin Reduced Amplitude Dressed Driving (RADD).

In Fig. 12(a), we plot the RMS values for TD, SATD, RADD and the uncorrected fields of H_{sym} [see Eq. (16)]. As our results show, there is there is a range of control loop times ($\Gamma t_0 > 8$) for which the control fields associated to the RADD dressing have an amplitude smaller than those of TD and SATD. Similarly to TD and SATD, RADD allows one to trace an eigenvalue braid that is not necessarily equivalent to the eigenvalue braid defined by H_{sym}, but still fulfills Eqs. (24) and (25), thus, generating a σ_x operation.

We can further reduce the amplitude of the control fields by choosing the base point of the control loop such that $\mathrm{Im}[\lambda_\pm]$ is anti-symmetric with respect to $t = t_0/2$, i.e., setting $\varphi = \pi$ and $\Omega_0 = \Gamma/2$ [see Sec.III B]. We compare in Fig. 12(b) the amplitudes of the field $\phi = \pi$, and find an overall reduction in the field amplitudes compared to Fig. 12(a), while still ensuring RADD produces fields smaller than SATD and TD.

To highlight the improvement in field amplitude of RADD compared to TD and SATD, we plot the absolute amplitudes for the control fields along the off-diagonal and diagonal elements of W_{STA} in Figs.12(c) and 12(d) respectively for TD, SATD, and RADD for $\Gamma t_0 = 8$ [see vertical purple line in Fig.12(a)] . The results highlight the impact RADD has on reducing filed amplitude.

In Fig. 11(c), this loop time corresponds to an average fidelity error of $\approx 10^{-5}$ when generating the σ_x swapping operation of the eigenvalues [see Eq. (25)] and tracing the eigenvalue braid associated to $H_{\mathrm{sym,RADD}}$.

However, for extremely short loop times the RMS values for the STAs grown polynomial relative to the uncorrected fields suggesting that the fields are so large compare to the uncorrected ones that it would be extremely difficult to realize such corrections in a given experimental setup. We surmise this behavior to be linked to the existence of a speed limit akin the quantum speed limit [59].

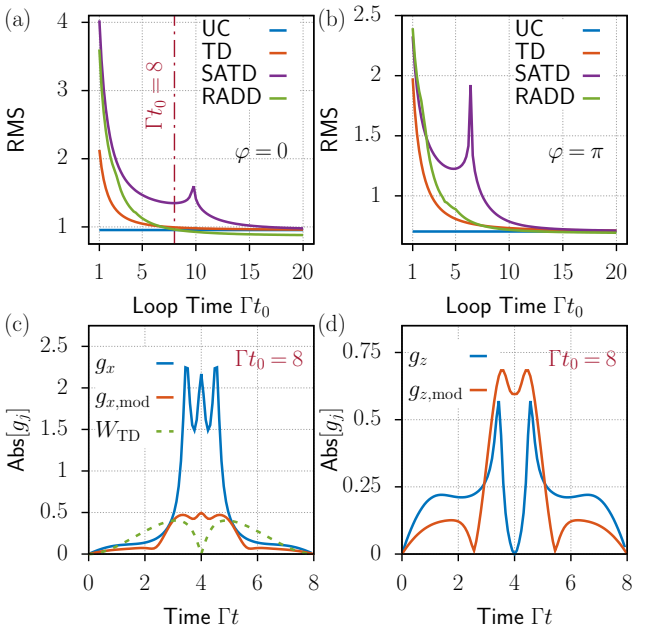

Figure 12. Comparison of resources needed to implement different STAs. (a) RMS as a function of Γt_0 for a circular control loop with base point at $\varphi = 0$ (b) Similar to (a), but with $\varphi = \pi$. (c) Absolute value of g_j for $j \in \{x, (x, \mathrm{mod})\}$ showing the overall improvement in field magnitude for $\Gamma t_0 = 8$ and $\varphi = 0$. (d) Same as (c) but for $j \in \{z, (z, \mathrm{mod})\}$. In (c), we plotted W_{TD} for comparison [see Eq. (35)].

Ultimately, we find that RADD allows one to generate an STA that is robust against parameter imprecisions and only requires moderate resources in terms of couplings and control field amplitudes, all while adhering to experimental constraints and reducing the magnitude of the control fields.

D. Experimentally Realizable STA Control

We now provide a generalized example of how one can construct an explicit STA control for an experimentally realized non-Hermitian Hamiltonian.

We start with a standard optomechanical setup with an additional laser tone given in [24], such that the system consists of two mechanical modes coupled linearly to two optical modes. Tracing out the degrees of freedom in the optical fields leads to the effective non-Hermitian Hamiltonian - which describes the evolution of the coupled modes that contains the exceptional points - pro-

duced below:

$$H = \sum_{j=1}^{2} \left[-\frac{1}{2}(\omega_j k - i\frac{\gamma_j}{2})\sigma_z + \eta_j(g_{2,j}^2 - g_{1,j}^2) \right] |j\rangle\langle j| - i\sum_{j=1}^{2} \eta_j g_{2,j} g_{1,j} \sigma_x, \tag{53}$$

where the j^{th} optical mode is coupled to the i^{th} mechanical mode using optomechanical couplings $g_{i,j}$ for $i, j \in 1, 2$. The optomechanical coupling rates for the mechanical modes are $g_{1,2}$, the mechanical mode coupling rates $\omega_{1,2}$, the mechanical damping rates $\gamma_{1,2}$, and

$$\eta_j = \frac{P_j}{\hbar\Omega_{\text{L},j}} \frac{\lambda_{\text{in},j}}{(\lambda_j/2)^2 + \Delta_j^2} \times \left[\frac{1}{\lambda_j/2 - i(2\omega_0 + \Delta_j)} - \frac{1}{\lambda_j/2 + i(2\omega_0 - \Delta_j)} \right], \tag{54}$$

where Δ_j is the mean detuning between the laser and the cavity, λ_j is the linewidth of the cavity, $\lambda_{\text{in},j}$ is the input coupling rate of the cavity, $\omega_0 = (\omega_1 + \omega_2)/2$, P_j is the power of the laser, and $\Omega_{\text{L},j}$ is its frequency. Note that the variables used here are taken directly from the paper, and for this section only they should be treated differently then their representations used in other sections of this paper.

H can be made time-dependent by making $\{P_j, \Delta_j\} \to \{P_j(t), \Delta_j(t)\}$, producing a Hamiltonian that structurally mirrors the time-dependant model used in H_{sym} [see Eq. (16)]. The straightforward approach to building $W(t)$ therefore involves comparing the coefficients of the modified optomechanical Hamiltonian $H_{\text{mod}} = H + W$, with those of the modified two-level non-Hermitian Hamiltonian $H_{\text{sym,STA}} = H_{\text{sym}} + W_{\text{STA}}$ by solving for the variables P_j and Δ_j in terms of Δ, and Ω. For this procedure, we assume from H_{sym} that $\{\Delta, \Gamma\} \in \mathbb{R}$, $\{\Omega, W_{\text{STA}}\} \in \mathbb{C}$, and all parameters in H [see Eq. (53)] are real as well.

Breaking H_{mod} and $H_{\text{sym,STA}}$ into their real and imaginary parts along σ_i for $i \in \{x, y, z\}$, and equating them with one another yields a system of equations that can be numerically solved for (but not analytically represented). The end result is an expression for $W(t)$ in terms of P_j and Δ_j in the same way W_{STA} can be expressed in terms of Δ and Ω. Finally we conclude our discussion of STAs by designing control fields for realized experimental systems that enforce desired behaviors such as topological eigenvalue braiding.

IV. CONCLUSION

In conclusion, we have demonstrated the effectiveness of different general dressed-state STA protocols in mimicking adiabatic dynamics when dynamically encircling an EP for a two-mode non-Hermitian system. Constructing these STAs for a non-Hermitian system must account for discontinuities present in the complex functions used to build the controls, otherwise the fields generated *may* not be usable. Additionally we found that a certain choice parameterization of the control loop and starting position along said loop can lead to near-adiabatic passage at precise times without STAs applied, giving us a quasi-coherent parameter regime which can be used to reduce the overall cost of the STA controls.

We used a well known Hermitian protocol known as transitionless driving (TD) which restored the ideal adiabatic dynamics (and traversed the ideal adiabatic braid) for all times. TD is resistant to the existence of branch cuts along its parameter loop, and can be made to work even with the discontinuities present. We found that TD always ensures braiding, but may not encircle the EP associated to the the modified Hamiltonian $H_{\text{sym,mod}}$. Using TD in the quasi-coherent regime reduces the overall energy of the control fields as well.

We also used super-adiabatic transitionless driving (SATD), which did not necessarily trace the ideal adiabatic braid, but produce the same end result. However, unlike in the Hermitian case, SATD for non-Hermitian systems may not work for all parameter sets; the dressing angle contains branch cuts that when accounted for, may break the condition needed for implementing the STA. Like TD, SATD always ensures braiding of the eigenvalues even if the modified EP is not encircled, and benefits from using the quasi-coherent regime.

Lastly we introduced a new STA known as reduced amplitude dressed driving (RADD) which improved the STA controls by greatly reducing the field amplitude. We found a range of loop times for which RADD produces smaller control fields than TD or SATD in the normal and quasi-coherent regimes. Finally, for all the STAs, we performed a robustness check when inserting a small imprecision into the system and find that the non-adiabatic dynamics return in the long time limit. However, a range of short loop times exist where the STAs are robust against the non-adiabatic errors.

[1] V. F. Krotov and I. N. Feldman, An iterative method for solving problems of optimal control, Engineering Cybernetics **21**, 123 (1983).

[2] J. Somlói, V. A. Kazakov, and D. J. Tannor, Controlled dissociation of I_2 via optical transitions between the X and B electronic states, Chem. Phys. **172**, 85 (1993).

[3] P. Doria, T. Calarco, and S. Montangero, Optimal control technique for many-body quantum dynamics, Phys. Rev. Lett. **106**, 190501 (2011).

[4] N. Khaneja, T. Reiss, C. Kehlet, T. Schulte-Herbrüggen,

and S. J. Glaser, Optimal control of coupled spin dynamics: design of NMR pulse sequences by gradient ascent algorithms, J. Magn. Reson. **172**, 296 (2005).
[5] S. J. Glaser, U. Boscain, T. Calarco, C. P. Koch, W. Köckenberger, R. Kosloff, I. Kuprov, B. Luy, S. Schirmer, T. Schulte-Herbrüggen, D. Sugny, and F. K. Wilhelm, Training Schrödinger's cat: quantum optimal control, Eur. Phys. J. D **69**, 279 (2015).
[6] S. Machnes, E. Assémat, D. Tannor, and F. K. Wilhelm, Tunable, flexible, and efficient optimization of control pulses for practical qubits, Phys. Rev. Lett. **120**, 150401 (2018).
[7] F. Motzoi, J. M. Gambetta, P. Rebentrost, and F. K. Wilhelm, Simple pulses for elimination of leakage in weakly nonlinear qubits, Phys. Rev. Lett. **103**, 110501 (2009).
[8] F. Motzoi, J. M. Gambetta, S. T. Merkel, and F. K. Wilhelm, Optimal control methods for rapidly time-varying Hamiltonians, Phys. Rev. A **84**, 022307 (2011).
[9] S. E. Economou and E. Barnes, Analytical approach to swift nonleaky entangling gates in superconducting qubits, Phys. Rev. B **91**, 161405 (2015).
[10] T. Figueiredo Roque, A. A. Clerk, and H. Ribeiro, Engineering fast high-fidelity quantum operations with constrained interactions, npj Quantum Information **7**, 10.1038/s41534-020-00349-z (2021).
[11] M. C. Rechtsman, Y. Lumer, Y. Plotnik, A. Perez-Leija, A. Szameit, and M. Segev, Topological protection of photonic path entanglement, Optica **3**, 925 (2016).
[12] S. Barik, A. Karasahin, C. Flower, T. Cai, H. Miyake, W. DeGottardi, M. Hafezi, and E. Waks, A topological quantum optics interface, Science **359**, 666 (2018).
[13] S. Mittal, E. A. Goldschmidt, and M. Hafezi, A topological source of quantum light, Nature **561**, 502 (2018).
[14] A. Blanco-Redondo, B. Bell, D. Oren, B. J. Eggleton, and M. Segev, Topological protection of biphoton states, Science **362**, 568 (2018).
[15] Y. Wang, X.-L. Pang, Y.-H. Lu, J. Gao, Y.-J. Chang, L.-F. Qiao, Z.-Q. Jiao, H. Tang, and X.-M. Jin, Topological protection of two-photon quantum correlation on a photonic chip, Optica **6**, 955 (2019).
[16] K. Tschernig, Á. Jimenez-Galán, D. N. Christodoulides, M. Ivanov, K. Busch, M. A. Bandres, and A. Perez-Leija, Topological protection versus degree of entanglement of two-photon light in photonic topological insulators, Nature Communications **12**, 1974 (2021).
[17] S. Mittal, V. V. Orre, E. A. Goldschmidt, and M. Hafezi, Tunable quantum interference using a topological source of indistinguishable photon pairs, Nature Photonics **15**, 542 (2021).
[18] T. Dai, Y. Ao, J. Bao, J. Mao, Y. Chi, Z. Fu, Y. You, X. Chen, C. Zhai, B. Tang, Y. Yang, Z. Li, L. Yuan, F. Gao, X. Lin, M. G. Thompson, J. L. O'Brien, Y. Li, X. Hu, Q. Gong, and J. Wang, Topologically protected quantum entanglement emitters, Nature Photonics **16**, 248 (2022).
[19] J. Deng, H. Dong, C. Zhang, Y. Wu, J. Yuan, X. Zhu, F. Jin, H. Li, Z. Wang, H. Cai, C. Song, H. Wang, J. Q. You, and D.-W. Wang, Observing the quantum topology of light, Science **378**, 966 (2022).
[20] K. Ding, C. Fang, and G. Ma, Non-Hermitian topology and exceptional-point geometries, Nature Reviews Physics **4**, 745 (2022).
[21] Y. S. S. Patil, J. Höller, P. A. Henry, C. Guria, Y. Zhang, L. Jiang, N. Kralj, N. Read, and J. G. E. Harris, Measuring the knot of non-Hermitian degeneracies and non-commuting braids, Nature **607**, 271 (2022).
[22] T. J. Milburn, J. Doppler, C. A. Holmes, S. Portolan, S. Rotter, and P. Rabl, General description of quasiadiabatic dynamical phenomena near exceptional points, Phys. Rev. A **92**, 052124 (2015).
[23] H. Ribeiro and F. Marquardt, Accelerated non-reciprocal transfer of energy around an exceptional point, arXiv (2021).
[24] H. Xu, D. Mason, L. Jiang, and J. Harris, Topological energy transfer in an optomechanical system with exceptional points, Nature **537**, 80 (2016).
[25] W. Liu, Y. Wu, C.-K. Duan, X. Rong, and J. Du, Dynamically encircling an exceptional point in a real quantum system, Phys. Rev. Lett. **126**, 170506 (2021).
[26] M. Abbasi, W. Chen, M. Naghiloo, Y. N. Joglekar, and K. W. Murch, Topological quantum state control through exceptional-point proximity, Phys. Rev. Lett. **128**, 160401 (2022).
[27] A. Baksic, H. Ribeiro, and A. A. Clerk, Speeding up adiabatic quantum state transfer by using dressed states, Phys. Rev. Lett. **116**, 230503 (2016).
[28] C. Guria, Q. Zhong, S. K. Ozdemir, Y. S. S. Patil, R. El-Ganainy, and J. G. E. Harris, Resolving the topology of encircling multiple exceptional points, Nature Communications **15**, 1369 (2024).
[29] S.-Y. Lee, J.-W. Ryu, S. W. Kim, and Y. Chung, Geometric phase around multiple exceptional points, Phys. Rev. A **85**, 064103 (2012).
[30] G. Demange and E.-M. Graefe, Signatures of three coalescing eigenfunctions, Journal of Physics A: Mathematical and Theoretical **45**, 025303 (2011).
[31] E. M. Graefe, U. GÃŒnther, H. J. Korsch, and A. E. Niederle, A non-hermitian symmetric bose-hubbard model: eigenvalue rings from unfolding higher-order exceptional points, Journal of Physics A: Mathematical and Theoretical **41**, 255206 (2008).
[32] K. Ding, Z. Q. Zhang, and C. T. Chan, Coalescence of exceptional points and phase diagrams for one-dimensional P T -symmetric photonic crystals, Phys. Rev. B **92**, 235310 (2015), arXiv:1509.07948 [physics.optics].
[33] J.-W. Ryu, S.-Y. Lee, and S. W. Kim, Analysis of multiple exceptional points related to three interacting eigenmodes in a non-hermitian hamiltonian, Phys. Rev. A **85**, 042101 (2012).
[34] K. Ding, G. Ma, M. Xiao, Z. Q. Zhang, and C. T. Chan, Emergence, coalescence, and topological properties of multiple exceptional points and their experimental realization, Phys. Rev. X **6**, 021007 (2016).
[35] E. Artin, Theory of braids, Annals of Mathematics **48**, 101 (1947).
[36] J. Höller, N. Read, and J. G. E. Harris, Non-hermitian adiabatic transport in spaces of exceptional points, Phys. Rev. A **102**, 032216 (2020).
[37] G. Nenciu, On the adiabatic theorem of quantum mechanics, Journal of Physics A: Mathematical and General **13**, L15 (1980).
[38] R. Uzdin, A. Mailybaev, and N. Moiseyev, On the observability and asymmetry of adiabatic state flips generated by exceptional points, Journal of Physics A: Mathematical and Theoretical **44**, 435302 (2011).
[39] M. V. Berry and R. Uzdin, Slow non-hermitian cycling: exact solutions and the stokes phenomenon, Journal of

Physics A: Mathematical and Theoretical **44**, 435303 (2011).
[40] J. W. Brown and R. V. Churchill, *Complex Variables and Applications*, eighth ed. (McGraw-Hill Higher Education, Boston, MA, 2009).
[41] A. Li, H. Wei, M. Cotrufo, W. Chen, S. Mann, X. Ni, B. Xu, J. Chen, J. Wang, S. Fan, C.-W. Qiu, A. Alù, and L. Chen, Exceptional points and non-hermitian photonics at the nanoscale, Nature Nanotechnology **18**, 706 (2023).
[42] Q. Zhong, M. Khajavikhan, D. N. Christodoulides, and R. El-Ganainy, Winding around non-hermitian singularities, Nature **9**, 4808 (2018).
[43] T. Dai, Y. Ao, J. Mao, Y. Yang, Y. Zheng, C. Zhai, Y. Li, J. Yuan, B. Tang, Z. Li, J. Luo, W. Wang, X. Hu, Q. Gong, and J. Wang, Non-hermitian topological phase transitions controlled by nonlinearity, Nature **20**, 101 (2024).
[44] R. El-Ganainy, K. G. Makris, M. Khajavikhan, Z. H. Musslimani, S. Rotter, and D. N. Christodoulides, Non-hermitian physics and pt symmetry, Nature **14**, 11 (2018).
[45] J. Yang, S. Shi, S. Yan, R. Zhu, X. Zhao, Y. Qin, B. Fu, X. Chen, H. Li, Z. Zuo, K. Jin, Q. Gong, and X. Xu, Non-orthogonal cavity modes near exceptional points in the far field, Communications Physics **7**, 13 (2024).
[46] J. del Pino, J. J. Slim, and E. Verhagen, Publisher correction: Non-hermitian chiral phononics through optomechanically induced squeezing, Nature **611**, E11 (2022).
[47] H.-K. Lau and A. A. Clerk, Fundamental limits and non-reciprocal approaches in non-hermitian quantum sensing, Nature Communications **9**, 4320 (2018).
[48] L. Huang, S. Huang, C. Shen, S. Yves, A. S. Pilipchuk, X. Ni, S. Kim, Y. K. Chiang, D. A. Powell, J. Zhu, Y. Cheng, Y. Li, A. F. Sadreev, A. Alù, and A. E. Miroshnichenko, Acoustic resonances in non-hermitian open systems, Nature Reviews Physics **6**, 11 (2024).
[49] J. Doppler, A. A. Mailybaev, J. Böhm, U. Kuhl, A. Girschik, F. Libisch, T. J. Milburn, P. Rabl, N. Moiseyev, and S. Rotter, Dynamically encircling an exceptional point for asymmetric mode switching, Nature **537**, 76–79 (2016).
[50] A. Wilkey, J. Suelzer, Y. N. Joglekar, and G. Vemuri, Theoretical and experimental characterization of non-markovian anti-parity-time systems, Communications Physics **6**, 308 (2023).
[51] W. Chen, Ş. Kaya Özdemir, G. Zhao, J. Wiersig, and L. Yang, Exceptional points enhance sensing in an optical microcavity, Nature **548**, 192 (2017).
[52] K. Y. Bliokh, D. Leykam, M. Lein, and F. Nori, Topological non-hermitian origin of surface maxwell waves, Nature Communications **10**, 580 (2019).
[53] I. I. Arkhipov, F. Minganti, A. Miranowicz, Şahin K. Özdemir, and F. Nori, Restoring adiabatic state transfer in time-modulated non-hermitian systems (2024), arXiv:2402.15298 [quant-ph].
[54] M. Demirplak and S. A. Rice, Adiabatic population transfer with control fields, The Journal of Physical Chemistry A **107**, 9937 (2003).
[55] M. Berry, Transitionless quantum driving, Journal of Physics A: Mathematical and Theoretical **42**, 365303 (2009).
[56] M. G. Bason, M. Viteau, N. Malossi, P. Huillery, E. Arimondo, D. Ciampini, R. Fazio, V. Giovannetti, R. Mannella, and O. Morsch, High-fidelity quantum driving, Nature Physics **8**, 147 (2012).
[57] M. Demirplak and S. Rice, On the consistency, extremal, and global properties of counterdiabatic fields, The Journal of chemical physics **129**, 154111 (2008).
[58] B. B. Zhou, A. Baksic, H. Ribeiro, C. G. Yale, F. J. Heremans, P. C. Jerger, A. Auer, G. Burkard, A. A. Clerk, and D. D. Awschalom, Accelerated quantum control using superadiabatic dynamics in a solid-state lambda system, Nature Physics **13**, 330 (2017).
[59] L. Mandelstam and I. Tamm, The uncertainty relation between energy and time in non-relativistic quantum mechanics, in *Selected Papers*, edited by B. M. Bolotovskii, V. Y. Frenkel, and R. Peierls (Springer Berlin Heidelberg, Berlin, Heidelberg, 1991) pp. 115–123.